

pubs.acs.org/joc Article

Photo-Click-Facilitated Screening Platform for the Development of Hetero-Bivalent Agents with High Potency

Lingyi Sun, Yongkang Gai, Christopher D. McNitt, Jun Sun, Xiaohui Zhang, Wei Xing, Zhonghan Li, Vladimir V. Popik, and Dexing Zeng*



Cite This: J. Org. Chem. 2020, 85, 5771–5777



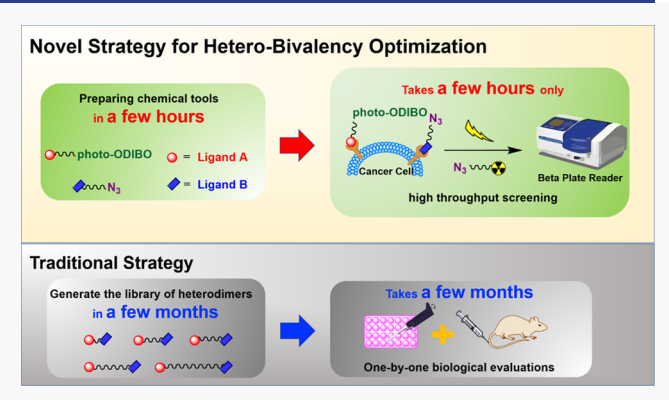
ACCESS

Metrics & More

Article Recommendations

Supporting Information

ABSTRACT: A novel photo-click-based platform has been developed for rapid screening and affinity optimization of heterobivalent agents. This method allows for the efficient selection of high-affinity dual receptor-targeting agents via streamlining tedious organic synthesis and biological evaluation procedures required by traditional approaches. The high-avidity heterobivalent agents targeting both integrin $\alpha_v \beta_3$ and urokinase-type plasminogen activator receptors have been developed using this photo-click-facilitated screening platform. The affinity screening results were further validated by traditional *in vitro* and *in vivo* evaluation techniques, reaffirming the reliability of the method. The convenience, rapidity, universality, and robustness of the screening platform, discussed in this report, can greatly facilitate the development of new heterobivalent agents for research and/or clinical applications.



■ INTRODUCTION

Heterobivalent agents, also known as dual receptor-targeting binders, consist of two linked ligands that simultaneously bind to two different receptors. 1,2 Dual receptor targeting has emerged as a highly promising strategy, as it provides several major advantages over the monoreceptor-targeting approach. First, heterobivalency can easily convert low-affinity monovalent ligands $(K_d \approx \mu M)$ into one with high avidity $(K_d \approx$ nM).3 Second, heterobivalency presents a new mechanism of action that is not available for monomers (or homodimers), and the second binding site can be a receptor with low density, low specificity, or even without specificity (such as a hydrophobic patch on a monomeric protein). Third, because of changes in size and lipophilicity, dual receptor-targeted ligands may also exhibit an improved pharmacokinetic performance, especially in cases where clearance properties and excretion rates are not optimal for monovalent counterparts.5-

Substantial efforts have been devoted to the development of heterobivalent agents for various biomedical applications. It has been widely recognized that the distance between two receptor-targeting ligands can dramatically affect the avidity of bivalent agents. Currently, to optimize the length of the linker between two targeting ligands, libraries of heterobivalent agents containing different linkers are prepared, and each agent in the library is individually evaluated *in vitro* and *in vivo* to select the most potent one(s). 11,112 However, such an approach

often involves multistep syntheses of library agents, ^{12–14} hindering their application in most biomedical research groups without extensive expertise in organic synthesis. In addition, individual testing and evaluation of every agent in the library usually take months, if not years. Furthermore, once the receptor(s) of interest changes, the entire library preparation/evaluation sequence has to be repeated again. Therefore, efficient screening of different length linkers between two receptor-targeting ligands remains the major unresolved challenge in the development of heterobivalent agents with high avidity. ^{13,15,16} Apparently, an efficient and robust strategy for rapid linker screening is highly desired by many biomedical research groups to utilize such a promising heterobivalent strategy in various biomedical applications.

Making use of the photo-triggered click chemistry ^{17,18} and radiochemical labeling, ^{19,20} we report a novel cell-based screening platform for facile linker optimization. This strategy allows for efficient selection of the most appropriate linker between ligands, while reducing the synthetic burden encountered during the optimization process. Compared to

Received: November 19, 2019 Published: March 30, 2020





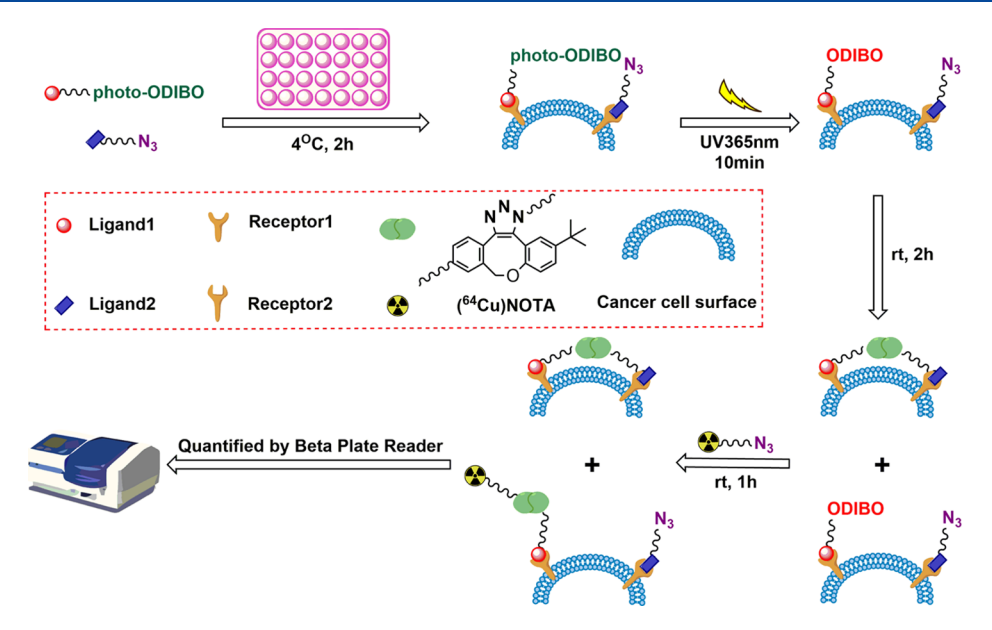


Figure 1. Illustration of the mechanism of the developed in vitro platform.

the traditional strategy discussed above, our cell-based strategy shortens the linker screening process. In addition, because of the high sensitivity of radioisotope techniques, ^{21,22} ligands are consumed on a nanomole scale in each test. Therefore, the cost associated with expensive starting materials (usually peptides^{23,24}) could also be significantly reduced. Considering the advantages of convenience, rapidity, sensitivity, and reliability, we believe that this universal and efficient screening platform will greatly facilitate the development of new heterobivalent pharmaceuticals for research and/or clinical applications.

This novel avidity optimization platform is based on the in situ formation of a heterodimer between two ligands that are simultaneously bound to two different receptors on the cell surface. Two ligands of interest can be derivatized with different PEGylated photo-oxa-dibenzocyclooctyne (photo-ODIBO) groups or azido groups $(-N_3)$ separately for the in situ formation of heterodimers containing different linkers. Herein, the photo-ODIBO group is a photo-triggered metalfree click chemistry moiety. Photo-ODIBO itself does not react with azide; upon UV irradiation (365 nm), it converts to ODIBO, which reacts with azides at a decent rate via strainpromoted alkyne-azide cycloaddition (SPAAC) (Scheme S1).25 To facilitate the use of this novel screening strategy in research groups lacking expertise in organic synthesis, the preparation of chemical tools has been designed in a way that does not involve complex protection/deprotection procedures and chromatography purifications. Without any further purification, the resulting chemical tools could be directly used in subsequent avidity optimization experiments.

The avidity optimization process is illustrated in Figure 1. Each well of cells was prefixed and incubated with one pair of ligands bearing specific PEGylated photo-ODIBO or N₃ for 2 h at 4 °C to allow sufficient binding of ligands to their receptors. Upon removal of excess (unbound) ligands, the plate can be irradiated with a 2 W hand-held UV lamp (365 nm) for 10 min to activate photo-ODIBO. After being incubated for an additional 2 h at room temperature (rt) to allow the completion of metal-free click reactions, a radio-scavenger such as (⁶⁴Cu)NOTA-N₃ can be added to click with the ODIBO remaining on cells. The amount of (⁶⁴Cu)NOTA-

N₃ clicked to the ODIBO is subsequently quantified using a MicroBeta2 Plate Counter. The well with the lowest radioactivity counts contains the least amount of remaining ODIBO and thus the highest amount of the *in situ*-generated heterodimer, indicating that the corresponding linker length will be most suitable for achieving high avidity.

RESULTS AND DISCUSSION

In our proof-of-principle study, two ligands of interest, RGD (targeting the integrin $\alpha \beta_3^{26,27}$) and AE105 [targeting the urokinase-type plasminogen activator receptor (uPAR)] 19,20 were selected for testing. Before conducting the avidity optimization via the strategy discussed above, the distance between one integrin $\alpha_{\nu}\beta_{3}$ receptor and one uPAR on the cell surface was estimated first to select the range of linker lengths for the screening. It was estimated that the distance between two receptors could be 60 Å or less (distance estimation is provided in the Supporting Information). Given the fact that the length of a single bond was around 1.5 Å, 28 the length of an extended PEG4 unit consisting of 12 single bonds would be around 15 Å if the bond angle is taken into account. Therefore, to cover the length up to 60 Å as well as to control the cost of this pilot study, four linkers consisting of PEG4, PEG8, PEG12, and PEG16 were selected for the screening purpose (Table 1).

Table 1. Linkers Selected for In Vitro Screening

entry	RGD	AE105	total	estimated length (Å)
1	PEG4	PEG0	PEG4	15
2	PEG4	PEG4	PEG8	30
3	PEG4	PEG8	PEG12	45
4	PEG4	PEG12	PEG16	60

As shown in Scheme S2, RGD-PEG4-photo-ODIBO was prepared by treating RGD with 6 equiv *N*,*N*-diisopropylethylamine (DIEA) and 3 equiv photo-ODIBO-PEG4-NHS. Highperformance liquid chromatography (HPLC) was used to monitor the progress of peptide modifications (see Supporting Information for HPLC conditions). Figure 2 shows the HPLC

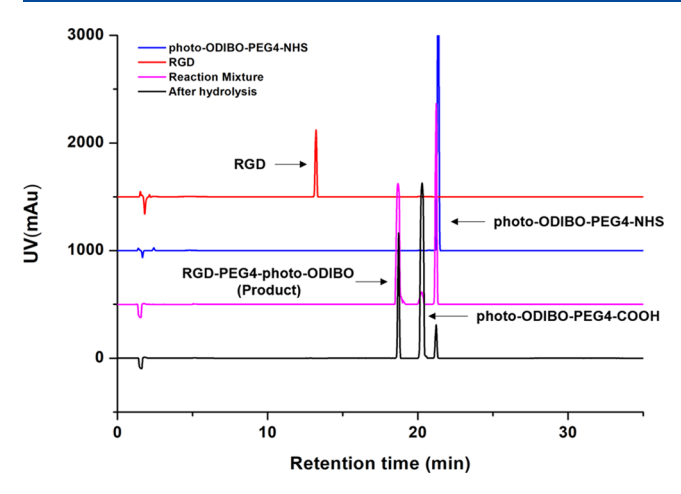


Figure 2. HPLC graphs of RGD functionalization. The RGD peak at 13 min (red trace) almost disappeared in the spectrum of the reaction mixture (pink trace) after 30 min incubation, indicating a highly efficient conversion from RGD to RGD-PEG4-photo-ODIBO. From the pink trace, the area of the photo-ODIBO-PEG4-NHS peak at 21 min was found to be over 20-fold that of the photo-ODIBO-PEG4-COOH peak at 20 min, indicating less than 5% hydrolysis.

chromatograms of reactions between photo-ODIOBO-PEG4-NHS and RGD, in which RGD, RGD-PEG4-photo-ODIBO, photo-ODIBO-PEG4-COOH, and photo-ODIBO-PEG4-NHS were eluted at 13, 19, 20, and 21 min, respectively. These HPLC data showed that after 30 min incubation at room temperature, the RGD conversion rate was over 98%, and less than 5% of photo-ODIBO-PEG4-NHS was hydrolyzed to photo-ODIBO-PEG4-COOH. Upon completing the peptide derivatization, 1× phosphate-buffered saline (PBS) was added to the reaction mixture to hydrolyze the excess photo-ODIBO-PEG4-NHS into photo-ODIBO-PEG4-COOH. After overnight incubation, the unreacted photo-ODIBO-PEG4-NHS was almost hydrolyzed to photo-ODIBO-PEG4-COOH, and thus only RGD-PEG4-photo-ODIBO and photo-ODIBO-PEG4-COOH existed in the resulting mixture. Parallel synthesis of AE105-PEGn-N₃ (2-5, n = 0, 4, 8, and 12) was conducted in the same manner by incubating AE105 with N₃-PEGn-NHS, followed by hydrolysis of excess NHS with 1× PBS (Figure S2). Because neither photo-ODIBO-PEG4-COOH nor N₃-PEGn-COOH would significantly bind to cells because of their lack of a targeting ligand, after being incubated with U87MG cells, they could be easily washed away together with those unbound RGD-PEG4-photo-ODIBO or AE105-PEGn-N₃. Therefore, the resulting reaction mixture can be directly applied in the subsequent cell-based avidity optimization experiments without any further purification.

Subsequently, four stock solutions, each containing a mixture of RGD-PEG4-photo-ODIBO with one of the AE105-PEGn-N $_3$ (n=0,4,8,12), were prepared. The four stock solutions were applied in the cell-based screening assay using prefixed U87MG cells (a human brain cancer cell line, overexpressing both the integrin $\alpha_v \beta_3$ receptor and uPAR and uPAR negative control group, in which cells were treated with RGD-PEG4-photo-ODIBO only, thus no heterodimer could be generated in this negative control group. Additionally, there was a background control group, in which no UV irradiation was applied, so that the amount of (64 Cu)NOTA-N $_3$ detected completely resulted from its nonspecific binding on cells. After

subtracting the nonspecific binding recorded in the background control group, the specific bindings of $(^{64}Cu)NOTA-N_3$ resulting from its ligation with RGD-PEG4-ODIBO in different groups were compared. As shown in Figure 3, the

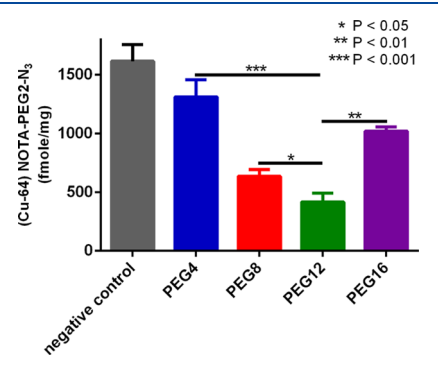


Figure 3. *In vitro* screening of selected linkers *via* the developed platform. (*, P < 0.05; **, P < 0.01; ***, P < 0.001). The negative control possesses the highest readout (1616.25) followed by PEG4 (1311.54), PEG16 (1021.21), PEG8 (635.073), and PEG12 (415.805), indicating that PEG12 is the most potent linker.

group treated with N_3 -PEG8-AE105 exhibited the least amount of specific binding of (64 Cu)NOTA- N_3 , suggesting that RGD-PEG12-AE105 was the most abundant heterodimer formed on U87MG cells, and the corresponding linker (entry 3) was the most potent one among the four tested linkers. The negative control group gave the highest counts, which could be attributed to the fact that all the activated RGD-PEG4-ODIBO was consumed by (64 Cu)NOTA- N_3 .

To validate the reliability of this newly developed avidity optimization strategy, the results obtained from the above screening assay were compared to those obtained from the traditional avidity optimization strategy by preparing the corresponding heterodimers and subsequently evaluating them individually both *in vitro* and *in vivo*.

In particular, the four RGD-AE105 heterodimers containing various PEG linkers (PEG4, PEG8, PEG12, and PEG16), which were previously reported by our group (Scheme S3), ¹² were then radiolabeled with either Cu-64 or Ga-68 for *in vitro* and *in vivo* evaluation, respectively.

Based on the Cu-64-based cell uptake results shown in Figure 4A, the PEG16- and PEG12-containing heterodimer exhibited the highest cell uptake, followed by PEG8- and PEG4-containing heterodimers with 4 h uptake values of 4.4, 3.8, 2.4, and 1.6% respectively. While in the cell efflux study (Figure 4B), the PEG8- and PEG12-containing heterodimers showed the best cell retention, followed by the PEG4-and PEG16-containing heterodimers with 2 h retention values of 69, 65, 54, and 36% respectively. Considering both the cell uptake and efflux results, among the four tested heterodimers, the PEG12-containing heterodimer demonstrated the highest overall performance, which is consistent with the results obtained from the above cell-based screening assay.

Further *in vivo* validation was conducted by comparing the Ga-68-based positron emission tomography (PET) imaging results obtained from mice bearing U87MG xenografts. As shown in Figure 5A, tumors could be visualized by using all the four tested heterodimeric PET tracers, while the PEG12-containing heterodimer exhibited the highest tumor to background contrast, followed by PEG8-, PEG16-, and PEG4-containing heterodimers. Quantitative tumor uptake

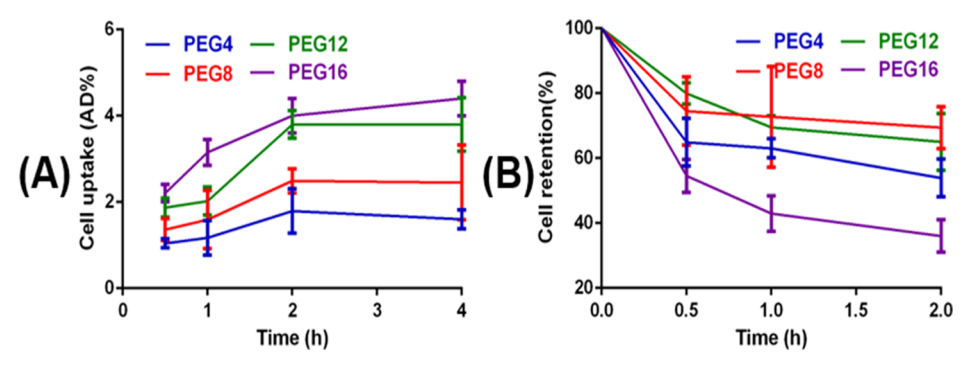


Figure 4. (A) Results of the Cu-64-based cell uptake study for heterodimers with various linkers, and (B) results of the cell efflux study for heterodimers with various linkers.

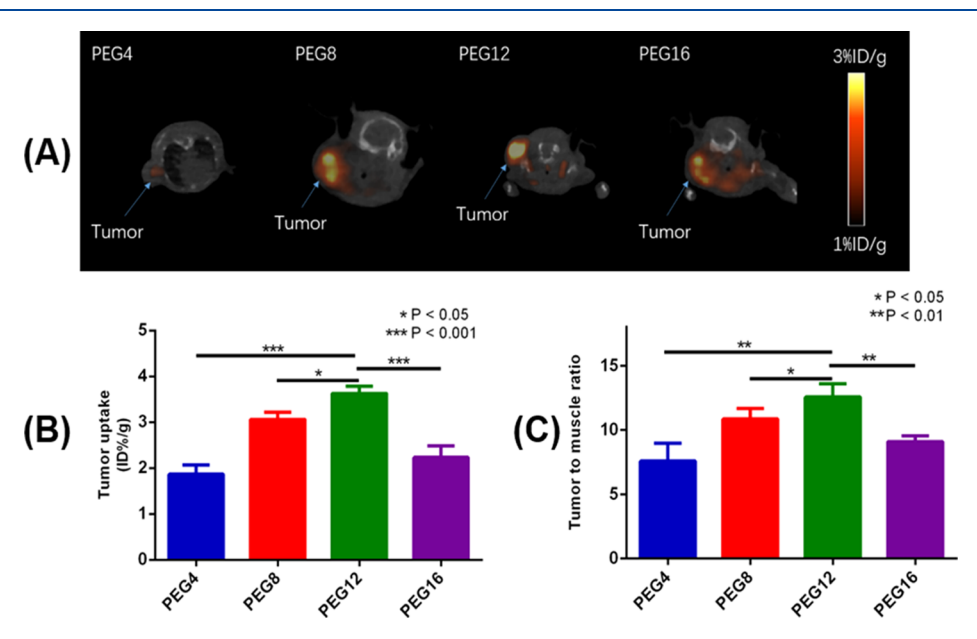


Figure 5. (A) PET imaging of the U87MG tumor using Ga-68 labeled heterodimers bearing the same length of linkers selected for *in vitro* screening. (B) Tumor uptake based on ROI quantification. (C) Tumor to muscle ratios based on ROI quantification. (*, P < 0.05; **, P < 0.01; ***, P < 0.001).

values were subsequently revealed by region of interest analysis (Figure 5B,C). The tumor uptake value of the PEG12-containing heterodimer was $3.63 \pm 0.15\%$ ID/g, while those of PEG8-, PEG16-, and PEG4-containing heterodimers were 3.01 ± 0.15 , 2.23 ± 0.25 , and $1.87 \pm 0.21\%$ ID/g, respectively. In addition, the heterodimer containing a PEG12 linker also showed a higher tumor/muscle ratio compared to heterodimers containing the other three linkers. Therefore, these *in vivo* evaluation results obtained from PET imaging were consistent with those results obtained from the above cell-based screening assay. Collectively, the results of both *in vitro* and *in vivo* evaluations successfully validated the accuracy and reliability of our developed rapid avidity optimization platform described above.

To conclude, utilizing a photo-triggered metal-free click reaction, we established the first universal *in vitro* screening platform for the rapid optimization of the ligand separation distance to achieve the high avidity of dual receptor targeting agents. This strategy can be broadly applied to various heterobivalent combinations and different diseases. The developed screening platform was successfully applied in the avidity optimization of the hetero-bivalent ligand that targets integrin $\alpha_v \beta_3$ -uPAR simultaneously. The reliability of this

platform was further validated by both *in vitro* and *in vivo* evaluations, in which heterodimers containing all the tested linkers were prepared and evaluated individually. The PEG12-containing heterodimer exhibited the best performance in both *in vitro* and *in vivo* evaluations, which was consistent with the results obtained from the designed cell-based screening assay, affirming the reliability of this platform. The demonstrated capability of performing the rapid screening using this universal platform makes us believe that it might significantly accelerate and enhance the applications of heterobivalency in various biomedical fields, particularly in the following situations: (1) when targeted receptors are expressed in low abundance and/ or (2) when high affinity (and/or specificity) monovalent ligands are not available.

■ EXPERIMENTAL SECTION

Materials and Equipment. Aqueous solutions were prepared using ultrapure water (resistivity, 18 M Ω ·cm). ⁶⁴Cu was obtained from Washington University (St. Louis, MO). ⁶⁸Ga (Eckert & Ziegler Isotope Products, Berlin, Germany) was eluted directly to a Modular-Lab (Eckert & Ziegler Isotope Products), concentrated on a Strata-X-C column from Phenomenex (Torrance, CA), and the ⁶⁸Ga-eluate was collected by desorbing it with 0.8 mL of 0.01 M HCl/98% acetone solution. All other chemicals were purchased from Sigma-

Aldrich Chemical Co. (St. Louis, MO) or Fisher Scientific (Pittsburgh, PA), unless otherwise specified. ESI-MS spectra were obtained on a Waters LCT-Premier XE LC-MS station (Milford, MA). Luna C-18 HPLC columns were from Phenomenex (Torrance, CA, USA). HPLC was performed on a Waters 1525 Binary HPLC pump (Milford, MA) with a Waters 2489 UV/visible detector and a model 106 Bioscan radioactivity detector for the purification of peptide conjugates and analysis of their radiolabeled conjugates using two elution buffers [0.1 vol % trifluoroacetic acid (TFA) in de-ionized water as elution buffer A and 0.1 vol % TFA in acetonitrile as elution buffer B]. PET/computed tomography (CT) data were acquired using an Inveon Preclinical Imaging Station (Siemens Medical Solutions).

Although the reaction mixture containing desired chemical tools could be used directly without any purification, we still have the product isolated to confirm its structure by LCMS.

Preparation of RGD-PEG4-Photo-ODIBO (1).

To 5 μ mol RGD and 15 μ mol photo-ODIBO PEG4 NHS in 500 μ L dimethyl sulfoxide (DMSO) was added 30 μ mol DIEA. The reaction mixture was allowed to stir at room temperature for 30 min. The product was then isolated via HPLC on a semipreparative C18 column using a gradient elution method [changing from 30% acetonitrile (ACN) to 70% ACN within 20 min at a flow rate of 4 mL/min]. The identity and purity of the isolated product were then characterized by high-resolution mass spectrometry (HRMS) as well as by reverse phase analytic HPLC (Figure S3). Yield 71%. HRMS (ESI-Orbitrap) m/z: [M + Na + H]²⁺/2; calcd for (C₅₆H₇₄N₉O₁₆Na/2): 575.7576; found: 575.7594.

Preparation of AE105-PEG0-N₃ (2).

To 5 μ mol AE105-NH₂ and 15 μ mol N₃-NHS in 500 μ L DMSO was added 30 μ mol DIEA. The reaction mixture was allowed to stir at room temperature for 30 min. The product was then isolated via HPLC on a semipreparative C18 column using a gradient elution method (changing from 20% ACN to 80% ACN within 20 min at a flow rate of 4 mL/min). The identity and purity of the isolated product were then characterized by HRMS as well as by reverse phase analytic HPLC (Figure S4). Yield 60%. HRMS (ESI-Orbitrap) m/z: [M + Na + H]²⁺/2; calcd for (C₆₄H₉₀N₁₇O₁₅Na/2): 679.8350; found: 679.8389.

Preparation of AE105-PEG4-N₃ (3).

To 5 μ mol AE105-NH₂ and 15 μ mol N₃-PEG4-NHS in 500 μ L DMSO was added 30 μ mol DIEA. The reaction mixture was allowed to stir at room temperature for 30 min. The product was then isolated via HPLC on a semipreparative C18 column using a gradient elution method (changing from 20% ACN to 80% ACN within 20 min at a flow rate of 4 mL/min). The identity and purity of the isolated product were then characterized by HRMS as well as by reverse phase analytic HPLC (Figure S5). Yield 67%. HRMS (ESI-Orbitrap) m/z: [M + Na + H]²⁺/2; calcd for (C₇₅H₁₁₁N₁₈O₂₀Na/2):, 803.4060; found: 803.4103.

Preparation of AE105-PEG8-N₃ (4).

To 5 μ mol AE105-NH₂ and 15 μ mol N₃-PEG8-NHS in 500 μ L DMSO was added 30 μ mol DIEA. The reaction mixture was allowed to stir at room temperature for 30 min. The product was then isolated via HPLC on a semipreparative C18 column using a gradient elution method (changing from 20% ACN to 80% ACN within 20 min at a flow rate of 4 mL/min). The identity and purity of the isolated product were then characterized by HRMS as well as by reverse phase analytic HPLC (Figure S6). Yield 73%. HRMS (ESI-Orbitrap) m/z: [M + Na + H]²⁺/2; calcd for (C₈₃H₁₂₇N₁₈O₂₄Na/2): 891.4584; found: 891.4640.

Preparation of AE105-PEG12-N₃ (5).

To 5 μ mol AE105-NH₂ and 15 μ mol N₃-PEG12-NHS in 500 μ L DMSO was added 30 μ mol DIEA. The reaction mixture was allowed to stir at room temperature for 30 min. The product was then isolated via HPLC on a semipreparative C18 column using a gradient elution method (changing from 20% ACN to 80% ACN within 20 min at a flow rate of 4 mL/min). The identity and purity of the isolated product were then characterized by HRMS as well as by reverse phase analytic HPLC (Figure S7). Yield 63%. HRMS (ESI-Orbitrap) m/z: [M + Na + H]²⁺/2; calcd for (C₉₁H₁₄₃N₁₈O₂₈Na/2): 979.5109; found: 980.0190.

Cell-Based Screening Assay for Linker Optimization. Cells were seeded on the 96-well plate (50,000 cells per well) with 1% bovine serum albumin (BSA) medium 24 h prior to the experiment. Upon being fixed by 4% paraformaldehyde for 30 min, the cells were subsequently incubated with 2 μ M RGD-PEG4-photo-ODIBO together with either 2 µM AE105-N₃ or AE105-PEG4-N₃ or AE105-PEG8-N3 or AE105-PEG12-N3 for 2 h at 4 °C using diluted reaction mixtures. A negative control group was also set up in which cells were treated with RGD-PEG4-photo-ODIBO together with NH₂-PEG4-AE105. Unbounded ligands were subsequently removed, and then cells were irradiated with 365 nm UV light for 10 min to activate the photo-ODIBO group to the clickable ODIBO group, resulting in on-site formation of the RGD-AE105 heterodimer via SPAAC between ODIBO on RGD and azide on AE105. After being incubated for additional 2 h, excess ⁶⁴Cu-labeled NOTA-PEG2-N₃ was added to photo-irradiated cells, which served as scavengers by reacting with unclicked ODIBO. Upon the removal of unreacted (64Cu)NOTA-PEG2-N₃, cells were treated with 1% sodium dodecyl sulfate (SDS), and the resulting lysed cells were immediately measured on a MicroBeta2 Plate Counter to quantify the amount of (64Cu)NOTA-PEG2-N3 attached on cells via SPAAC with RGD-PEG4-ODIBO.

Cell Uptake Study. Cells were seeded in 12-well plates (200,000 cells per well) 24 h prior to the experiment. Before the experiment, the cells were washed with 1 mL Hanks' balanced salt solution (HBSS) twice, and 1 mL media [Dulbecco's modified Eagle medium (DMEM) with 0.1% BSA and 1 mM Mn²⁺] was added to each well. Cells were then incubated with ⁶⁴Cu-labeled conjugates (10 pmol per well) with and without the addition of an excess blocking agent (10 μ g AE105 + 10 μ g RGD) to determine the nonspecific uptake. At each time point (1, 2, and 4 h), radioactive media were aspirated. The cells were washed twice with HBSS (pH 7.2) and dissolved in 0.5% SDS. The radioactivity of each cell lysate sample was measured using a gamma counter. The protein content of each cell lysate sample was determined. The measured radioactivity associated with each cell

lysate sample was normalized to the amount of cell protein present. The cell uptake was expressed as the percentage added dose after decay correction.

Cell Efflux Study. Cells were seeded in a 12-well plate 24 h prior to the experiment. Cells were incubated with 64 Cu-labeled conjugates (10 pmol per well) in culturing media contained 1 mM MnCl $_2$ for 2 h at 37 °C. Media were then removed and cells were washed twice with HBSS. Fresh media without MnCl $_2$ were then added to the cells. At 0, 30, 60, and 120 min following fresh media, addition cells were washed twice and dissolved in 0.5% SDS. The activity was measured using a gamma counter. Cell retention values at different time points were calculated by dividing the cell retention at that time point with cell retention at 0 min.

Small Animal PET/CT Imaging Studies. 68 Ga-labeling of various heterodimers was conducted by incubating heterodimers and 68 Ga in 0.1 M NaOAc buffer (pH \approx 4.0) at 90 °C for 10 min, with a specific activity of 37 Mbq/nmol. All animal studies were conducted under a protocol approved by the University of Pittsburgh Institutional Animal Care and Use Committee. U87MG xenograft tumor-bearing mice were injected intravenously (lateral tail vein) with prepared 68 Ga-labeled heterodimers (3.7 Mbq/mice). At 1 h postinjection, mice were anesthetized with 2% isoflurane, and small animal PET/CT was performed. Static images were collected for 15 min. PET and CT images were co-registered with Inveon Research Workstation (IRW) software (Siemens Medical Solutions). PET images were reconstructed with the 3-dimensional ordered-subsets expectation maximization /maximum a posteriori probability algorithm, and the analysis of images was done using IRW.

ASSOCIATED CONTENT

Solution Supporting Information

The Supporting Information is available free of charge at https://pubs.acs.org/doi/10.1021/acs.joc.9b03122.

Distance estimation between the receptors and HPLC conditions (PDF)

AUTHOR INFORMATION

Corresponding Author

Dexing Zeng — Department of Radiology, University of Pittsburgh, Pittsburgh, Pennsylvania 15213, United States; Department of Diagnostic Radiology, Oregon Health & Science University, Portland, Oregon 97239, United States; orcid.org/0000-0003-4948-5275; Email: zengd@ohsu.edu

Authors

Lingyi Sun — Department of Radiology, University of Pittsburgh, Pittsburgh, Pennsylvania 15213, United States; Department of Diagnostic Radiology, Oregon Health & Science University, Portland, Oregon 97239, United States; orcid.org/0000-0003-2111-8764

Yongkang Gai — Department of Radiology, University of Pittsburgh, Pittsburgh, Pennsylvania 15213, United States; orcid.org/0000-0001-6766-5240

Christopher D. McNitt – Department of Chemistry, University of Georgia, Athens, Georgia 30602, United States

Jun Sun – Department of Radiology, University of Pittsburgh, Pittsburgh, Pennsylvania 15213, United States; Department of Radiology, Third Affiliated Hospital of Suzhou University, Changzhou, Jiangsu 213003, China

Xiaohui Zhang — Department of Radiology, University of Pittsburgh, Pittsburgh, Pennsylvania 15213, United States Wei Xing — Department of Radiology, Third Affiliated Hospital of Suzhou University, Changzhou, Jiangsu 213003, China **Zhonghan Li** — Department of Diagnostic Radiology, Oregon Health & Science University, Portland, Oregon 97239, United States

Vladimir V. Popik — Department of Chemistry, University of Georgia, Athens, Georgia 30602, United States;

ocid.org/
0000-0001-9112-3935

Complete contact information is available at: https://pubs.acs.org/10.1021/acs.joc.9b03122

Author Contributions

¹L.S. and Y.G. contributed equally.

Notes

The authors declare no competing financial interest.

ACKNOWLEDGMENTS

We thank Kathryn Elizabeth Day and Joseph Donald Latoche for their assistance in PET imaging studies. This work was supported by the National Institute of Biomedical Imaging and Bioengineering grants R21-EB017317 and R21-EB020737 and American Cancer Society Research Scholar (no. ACS-RSG-17-004-01-CCE). Preclinical PET/CT imaging was supported in part by P30CA047904 (UPCI CCSG). The development of photo-SPAAC reagents was supported by NSF (CHE-1565646).

REFERENCES

- (1) Mammen, M.; Choi, S.-K.; Whitesides, G. M. Polyvalent Interactions in Biological Systems: Implications for Design and Use of Multivalent Ligands and Inhibitors. *Angew. Chem., Int. Ed.* **1998**, *37*, 2754–2794.
- (2) Mulder, A.; Huskens, J.; Reinhoudt, D. N. Multivalency in supramolecular chemistry and nanofabrication. *Org. Biomol. Chem.* **2004**, *2*, 3409–3424.
- (3) Krishnamurthy, V. M.; Estroff, L. A.; Whitesides, G. M. Multivalency in Ligand Design. *Fragment-Based Approaches in Drug Discovery*; Wiley-VCH Verlag GmbH & Co. KGaA, 2006; Vol. 11–53.
- (4) Jain, A.; Whitesides, G. M.; Alexander, R. S.; Christianson, D. W. Identification of two hydrophobic patches in the active-site cavity of human carbonic anhydrase II by solution-phase and solid-state studies and their use in the development of tight-binding inhibitors. *J. Med. Chem.* 1994, 37, 2100–2105.
- (5) Durkan, K.; Jiang, Z.; Rold, T. L.; Sieckman, G. L.; Hoffman, T. J.; Bandari, R. P.; Szczodroski, A. F.; Liu, L.; Miao, Y.; Reynolds, T. S.; Smith, C. J. A heterodimeric [RGD-Glu-[(64)Cu-NO2A]-6-Ahx-RM2] alphavbeta3/GRPr-targeting antagonist radiotracer for PET imaging of prostate tumors. *Nucl. Med. Biol.* **2014**, *41*, 133–139.
- (6) Xu, L.; Josan, J. S.; Vagner, J.; Caplan, M. R.; Hruby, V. J.; Mash, E. A.; Lynch, R. M.; Morse, D. L.; Gillies, R. J. Heterobivalent ligands target cell-surface receptor combinations in vivo. *Proc. Natl. Acad. Sci. U.S.A.* **2012**, *109*, 21295–21300.
- (7) Kuil, J.; Buckle, T.; Oldenburg, J.; Yuan, H.; Borowsky, A. D.; Josephson, L.; van Leeuwen, F. W. B. Hybrid peptide dendrimers for imaging of chemokine receptor 4 (CXCR4) expression. *Mol. Pharm.* **2011**, *8*, 2444–2453.
- (8) Li, Z.-B.; Wu, Z.; Chen, K.; Ryu, E. K.; Chen, X. 18F-labeled BBN-RGD heterodimer for prostate cancer imaging. *J. Nucl. Med.* **2008**, *49*, 453–461.
- (9) Rojo, J. Synthetic Multivalent Molecules. Concepts and Biomedical Applications. By Seok-Ki Choi. *Angew. Chem., Int. Ed.* **2005**, *44*, 2629–2630.
- (10) Fan, E.; Zhang, Z.; Minke, W. E.; Hou, Z.; Verlinde, C. L. M. J.; Hol, W. G. J. High-Affinity Pentavalent Ligands of Escherichia coli Heat-Labile Enterotoxin by Modular Structure-Based Design. *J. Am. Chem. Soc.* **2000**, 122, 2663–2664.
- (11) Kitov, P. I.; Shimizu, H.; Homans, S. W.; Bundle, D. R. Optimization of tether length in nonglycosidically linked bivalent

- ligands that target sites 2 and 1 of a Shiga-like toxin. J. Am. Chem. Soc. 2003, 125, 3284–3294.
- (12) Gai, Y.; Xiang, G.; Ma, X.; Hui, W.; Ouyang, Q.; Sun, L.; Ding, J.; Sheng, J.; Zeng, D. A Universal Molecular Scaffold for Facile Construction of Multivalent and Multimodal Imaging Probes. *Bioconjugate Chem.* **2016**, *27*, 515–520.
- (13) Yan, Y.; Chen, X. Peptide heterodimers for molecular imaging. *Amino Acids* **2011**, *41*, 1081–1092.
- (14) Luo, H.; Hong, H.; Yang, S. P.; Cai, W. Design and applications of bispecific heterodimers: molecular imaging and beyond. *Mol. Pharm.* **2014**, *11*, 1750–1761.
- (15) Kane, R. S. Thermodynamics of Multivalent Interactions: Influence of the Linker. *Langmuir* **2010**, *26*, 8636–8640.
- (16) Krishnamurthy, V. M.; Semetey, V.; Bracher, P. J.; Shen, N.; Whitesides, G. M. Dependence of Effective Molarity on Linker Length for an Intramolecular Protein–Ligand System. *J. Am. Chem. Soc.* **2007**, *129*, 1312–1320.
- (17) Poloukhtine, A. A.; Mbua, N. E.; Wolfert, M. A.; Boons, G.-J.; Popik, V. V. Selective Labeling of Living Cells by a Photo-Triggered Click Reaction. *J. Am. Chem. Soc.* **2009**, *131*, 15769–15776.
- (18) Arumugam, S.; Popik, V. V. Sequential "Click" "Photo-Click" Cross-Linker for Catalyst-Free Ligation of Azide-Tagged Substrates. *J. Org. Chem.* **2014**, *79*, 2702–2708.
- (19) Sun, L.; Gai, Y.; Anderson, C. J.; Zeng, D. Highly-efficient and versatile fluorous-tagged Cu(i)-catalyzed azide-alkyne cycloaddition ligand for preparing bioconjugates. *Chem. Commun.* **2015**, *51*, 17072–17075.
- (20) Sun, L.; Ding, J.; Xing, W.; Gai, Y.; Sheng, J.; Zeng, D. Novel Strategy for Preparing Dual-Modality Optical/PET Imaging Probes via Photo-Click Chemistry. *Bioconjugate Chem.* **2016**, *27*, 1200–1204.
- (21) Wadas, T.; Wong, E.; Weisman, G.; Anderson, C. Copper chelation chemistry and its role in copper radiopharmaceuticals. *Curr. Pharm. Des.* **2007**, *13*, 3–16.
- (22) Williams, H. A.; Robinson, S.; Julyan, P.; Zweit, J.; Hastings, D. A comparison of PET imaging characteristics of various copper radioisotopes. *Eur. J. Nucl. Med. Mol. Imag.* **2005**, *32*, 1473–1480.
- (23) Lee, S.; Xie, J.; Chen, X. Peptide-Based Probes for Targeted Molecular Imaging. *Biochemistry* **2010**, *49*, 1364–1376.
- (24) Chen, K.; Conti, P. S. Target-specific delivery of peptide-based probes for PET imaging. *Adv. Drug Deliv. Rev.* **2010**, *62*, 1005–1022.
- (25) McNitt, C. D.; Popik, V. V. Photochemical generation of oxadibenzocyclooctyne (ODIBO) for metal-free click ligations. *Org. Biomol. Chem.* **2012**, *10*, 8200–8202.
- (26) Danhier, F.; Le Breton, A.; Préat, V. RGD-based strategies to target alpha(v) beta(3) integrin in cancer therapy and diagnosis. *Mol. Pharm.* **2012**, *9*, 2961–2973.
- (27) Chen, K.; Chen, X. Integrin Targeted Delivery of Chemotherapeutics. *Theranostics* **2011**, *1*, 189–200.
- (28) Bartell, L. S. On the Length of the Carbon-Carbon Single Bond. *J. Am. Chem. Soc.* **1959**, *81*, 3497–3498.
- (29) Maschauer, S.; Haubner, R.; Kuwert, T.; Prante, O. (18)F-glyco-RGD peptides for PET imaging of integrin expression: efficient radiosynthesis by click chemistry and modulation of biodistribution by glycosylation. *Mol. Pharm.* **2014**, *11*, 505–515.
- (30) Li, Z.-B.; Niu, G.; Wang, H.; He, L.; Yang, L.; Ploug, M.; Chen, X. Imaging of urokinase-type plasminogen activator receptor expression using a 64Cu-labeled linear peptide antagonist by microPET. Clin. Cancer Res. 2008, 14, 4758–4766.